



Contents lists available at ScienceDirect

Earth and Planetary Science Letters

journal homepage: www.elsevier.com/locate/epsl

Topography of Mars from global mapping by HRSC high-resolution digital terrain models and orthoimages: Characteristics and performance

K. Gwinner^{a,*}, F. Scholten^a, F. Preusker^a, S. Elgner^a, T. Roatsch^a, M. Spiegel^b, R. Schmidt^c, J. Oberst^a, R. Jaumann^a, C. Heipke^c

^a Institute of Planetary Research, German Aerospace Center (DLR), Rutherfordstr. 2, D-12489 Berlin, Germany

^b Photogrammetry and Remote Sensing, Technische Universität München, Arcisstr. 21, D-80333 München, Germany

^c Institute of Photogrammetry and Geoinformation, Leibniz Universität Hannover, Nienburger Str. 1, D-30167 Hannover, Germany

ARTICLE INFO

Article history:

Accepted 2 November 2009

Available online xxx

Keywords:

Mars
global planetary mapping
stereo imaging
digital terrain model
orthoimage

ABSTRACT

We report on the results of the Mars Express High-Resolution Stereo Camera (HRSC) experiment pertaining to one of its major aims, mapping the surface of Mars by high-resolution digital terrain models (DTM, up to 50 m grid spacing) and orthoimages (up to 12.5 m resolution). We introduce the specifications and characteristics of these data products and give an overview of the procedures that have been developed and are applied for their derivation. We also address the performance characteristics of the mapping project related to different aspects of internal accuracy, accuracy with respect to the global reference system, and regional aspects. Using adaptive processing techniques for terrain reconstruction and a revised approach to the improvement of orientation data, a mean precision of the resulting 3D points of about 12 m is obtained, exceeding the mean ground resolution of the stereo images. Using Mars Orbiter Laser Altimeter (MOLA) data, the HRSC models are firmly tied to the global reference system at the scale of the HRSC DTM grid spacing in the lateral dimension, and to within few meters vertically. HRSC high-resolution DTMs are typically generated using a grid size of about 2 times the mean ground resolution, but usually not larger than 3 times the mean ground resolution, and not smaller than 3 times the precision of the integrated 3D points derived from stereo image analysis. Statistically, every grid cell is based on at least one measured 3D point. Thus, horizontal DTM resolution is well established with regard to the precision and density of the derived 3D points, while the concurrent aim of a detailed terrain representation at maximum possible resolution is pursued. Comparison with the DTM derived from MOLA data allows us to identify specific advancements related to this updated view of Martian topography. We also address the mapping performance of HRSC in comparison to MOLA with respect to latitude and to different surface types and morphologies. Finally, comparison with MOLA highlights typical complementarities of the two different approaches for mapping planetary surfaces.

© 2009 Elsevier B.V. All rights reserved.

1. Introduction

Detailed mapping of topography is central to the understanding of the processes shaping the surfaces of the planets. For Mars, extensive earlier topographic mapping efforts were based on image data obtained by the Viking Orbiter spacecraft (Snyder, 1979; Wu and Doyle, 1990), and in particular on manual measurements by operators (Greeley and Batson, 1990). With increased availability of computer power, also digital models have been derived, mainly with resolutions at km-scale, and higher resolution was achieved in local areas (Thornhill et al., 1993). As emphasis was on completeness of the

surface coverage as such, much of the stereo coverage of Viking was obtained only by chance.

Accurate surface topography was obtained by the Mars Orbiter Laser Altimeter (MOLA) instrument on Mars Global Surveyor (Smith et al., 2001). MOLA heights are observed along separate measurement profiles, in contrast to the area-based approach represented by stereo imaging. MOLA profiles provide a vertical accuracy on the order of meters, depending on signal quality and terrain roughness, and a horizontal uncertainty of smaller than 100 m (Neumann et al., 2003). MOLA surface spots have a nominal diameter of 168 m from 400 km orbit height, and a shot spacing of 300 m (Smith et al., 2001). The individual measurement tracks overlap near the poles, but gaps between tracks amount to about 4 km near the equator. For the global raster DTM product (1/128° raster, i.e. 463 m grid spacing at the equator, PDS dataset MGS-M-MOLA-5-MEGDR-L3-V1.0, <http://pds-geosciences.wustl.edu/missions/mgs/megdr.html>), a horizontal

* Corresponding author. Tel.: +49 30 67055 310; fax: +49 30 67055 402.

E-mail address: Klaus.Gwinner@dlr.de (K. Gwinner).

accuracy of about 200 m and a vertical accuracy on the order of 10 m can be expected on average.

The High-Resolution Stereo Camera (HRSC; Neukum et al., 2004; Jaumann et al., 2007) onboard the European mission Mars Express (MEX) is the first planetary sensor system which has a built-in stereo functionality and is specifically designed for photogrammetric mapping. HRSC is a multi-line pushbroom stereo camera providing up to 5 panchromatic multi-angle observations of the surface during each Mars orbit. Simultaneously, multi-spectral imagery is acquired by four CCD lines equipped with spectral filters (near-infrared, red, green, blue). A nominal ground resolution of up to 10 m/pixel is achieved. Beyond stereo capability, HRSC data are unique since a single imaging sequence covers very large areas (typically on the order of 10^4 – 10^5 km²) at high image resolution. By imaging sequence we denote the set of synchronous HRSC stereo and color images for the same ground track. The capability of simultaneous acquisition of stereo imagery avoids the difficulties related to changes of imaging conditions which may occur between successive orbital passes and makes pointing maneuvers for obtaining stereo coverage unnecessary.

Recently, stereo imagery of even higher resolution has become available. Mars Global Surveyor has provided stereoscopic coverage with its wide-angle camera at 225 m/pixel and stereo coverage by its narrow-angle device for selected areas of interest (Malin and Edgett, 2001; Kirk et al., 2003; Yoon and Shan, 2005). The HiRISE experiment onboard Mars Reconnaissance Orbiter is acquiring stereo imagery for ~0.1% of the surface at meter-scale resolution (McEwen et al., 2007; Kirk et al., 2007). Stereo coverage is obtained by tilting the spacecraft in consecutive orbits in both cases. However, because of the lack in lateral coverage, the data do not provide the basis for a global mapping attempt.

In this paper we address the achievements of the HRSC experiment onboard Mars Express (Neukum et al., 2004) relative to the global mapping of the topography of Mars by high-resolution DTMs and orthoimages. These data products are also called Level-4 products, according to HRSC experiment nomenclature. After a preparatory phase that was dedicated to the performance analysis and refinement of HRSC 3D processing (Heipke et al., 2004; Albertz et al., 2005; Gwinner et al., 2005, 2009; Scholten et al., 2005; Kirk et al., 2006; Spiegel, 2007a,b) and comparison with alternative approaches to HRSC photogrammetric processing (Heipke et al., 2007), a mapping program for systematic derivation of HRSC Level-4 products has been established and started at the German Aerospace Center (DLR) in 2007 (Gwinner et al., 2008).

The purpose of this paper is to introduce the general specifications of the HRSC high-level photogrammetric data products for Mars and to give an overview of the procedures applied for their derivation. Among the different methods involved (Gwinner et al., 2009), the presentation of the procedure for improvement of exterior orientation data, some aspects of which have not been described previously, is addressed in more detail. We will then analyze the performance characteristics of the overall mapping project related to image resolution, absolute accuracy, the internal accuracy of the DTMs, i.e. the level of detail achieved by the topographic reconstruction, and corresponding regional aspects. Finally, we derive some general conclusions with respect to the updated view of Martian topography, and its comparison with the existing global DTM derived from laser altimetry profiles of the MOLA instrument. Comparison of MOLA results with HRSC DTMs is of specific interest also because of the current trend in planetary exploration to include both, laser instruments and imaging sensors with stereo capabilities for orbiter missions (e.g. Selene, Messenger, Lunar Reconnaissance Orbiter, BepiColombo).

2. HRSC data properties and coverage

Photogrammetric analysis of HRSC data uses so-called Level-2 data, i.e. decompressed and radiometrically calibrated imagery

(Jaumann et al., 2007). The radiometric calibration of the image data comprises flat-fielding and absolute flux calibration. The geometric calibration parameters of the camera have been determined from laboratory measurements before the launch (Jaumann et al., 2007) and have been checked and improved based on HRSC data from orbit (Spiegel, 2007b). Using 46 selected orbits systematic errors in the image coordinates of the tie-points have been removed by improving the coordinates x_0, y_0 of the focal point in a self-calibrating bundle adjustment, i.e. the parameters of the exterior orientation and the coordinates of the focal point were determined simultaneously.

The image data are also amended by orbit and pointing data. These base data are available via the PSA (Planetary Science Archive) and PDS (Planetary Data System) catalogues (<http://www.rssd.esa.int/PSA>, http://pds-geosciences.wustl.edu/missions/mars_express/hrsc.htm).

HRSC imagery is compressed onboard by a lossy, JPEG-based discrete cosine transform (DCT) compression with average compression factors of 4–40 that affects the effective ground resolution of the images (Jaumann et al., 2007; Gwinner et al., 2009). Permanent effects of compression on the images comprise image block artifacts (through separate compression of non-overlapping 8×8 image windows) and manipulation of the spectral domain by encoding transform parameters with reduced accuracy. Compression effects are stronger on low-contrast areas and need to be specifically addressed during the process of DTM generation in order to reduce errors (see Section 4.2 and Gwinner et al., 2009).

In addition to Level-2 data and Level-4 data (HRSC high-resolution DTMs and orthoimages), so-called Level-3 data are available. These are map projected image data, but rectification is based on the terrain representation provided by the MOLA DTM, not on higher-resolution HRSC DTM (see Section 4.3).

At the time of writing, the derivation of HRSC high-resolution DTMs and orthoimages for the complete HRSC dataset is an ongoing process, as is the mission itself. Currently, HRSC nadir channel data acquired by the regional mapping mode cover 115 million km², or about 79.3% of the surface of Mars. The datasets considered in Sections 5 and 6 comprise all imaging sequences for which the processing has been finished before December 2008. The highest respective MEX orbit number is 2217, which is close to the end of the nominal mission phase (2004–2005). Thus, the available product datasets already allow us to assess the mapping performance of HRSC from a global perspective, since they cover a substantial fraction of the surface of Mars, the full latitude range, and the full range of typical mean ground resolutions of the HRSC stereo channels (Fig. 1). Note that, because of limitations to data volume, HRSC stereo images are often acquired with lower resolution than the nadir channel images.

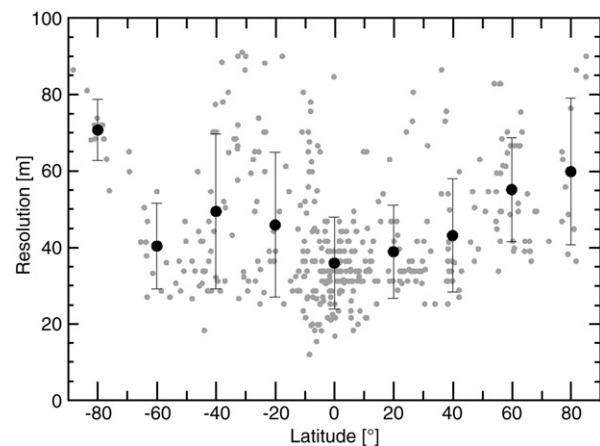


Fig. 1. Mean HRSC stereo image ground resolution vs. latitude of the center of the image sequence. Local averages and standard deviations are indicated. Only stereo imaging sequences corresponding to the HRSC high-resolution DTM and orthoimage datasets considered in this paper are shown.

Table 1
Overview of the main HRSC Level-4 data product specifications.

	DTM	Orthoimage
Product subtypes	Spheroid DTM Areoid DTM	Panchromatic (nadir), red, green, blue and near-infrared channel orthoimages
Data format	16 bit, numeric height resolution 1 m	8 bit
Spatial resolution	50 m/75 m/100 m/... depending on quality of image and orientation data	12.5 m/25 m/50 m... depending on ground resolution
Reference bodies for height	Spheroid $r = 3396$ km and GMM3-derived equipotential surface (areoid DTM)	n/a
Ref. body for map projection	Spheroid $r = 3396$ km	Spheroid $r = 3396$ km
Map projection	Sinusoidal ($\pm 85^\circ$ latitude) Polar-Stereographic (polar areas)	Sinusoidal ($\pm 85^\circ$ latitude) Polar-Stereographic (polar areas)

3. HRSC Level-4 product specifications and PDS specifications

The data products of the systematic HRSC Level-4 processing (Table 1) are 8 bit orthoimages for the nadir channel and the 4 color channels and 16 bit DTMs (1 m numeric height resolution). They are originally created in VICAR format (see Scholten et al., 2005) and then formatted according to PDS specifications. The map scales of the orthoimages adhere to standard resolutions (12.5, 25, 50... m/pixel), depending on the ground resolution of the respective image. For the specification of the DTM spatial resolution, the quality of image and orientation data is also decisive (see Section 5.2). Most frequently, a grid spacing of about 2 times the mean stereo resolution can be used (up to 50 m). The principal geometric reference for both planimetry and height is a sphere of radius $r = 3396.0$ km as defined by the MOLA team (Smith et al., 2001). In addition to the spheroid DTM, an areoid DTM is produced. Again in agreement with the datum used by the MOLA team, the areoid DTM represents heights above an equipotential surface described by the potential model GMM3 (PDS dataset MGS-M-MOLA-5-MEGDR-L3-V1.0). The areoid is the Martian analog to the geoid known in terrestrial geodesy. Being referred to the gravity potential field, the areoid DTM may better serve the purposes of specific geoscientific studies, e.g. those addressing gravity-driven processes or regional slope angles. On the other hand, due to its simple and entirely geometric definition, the spheroid reference system allows for straightforward transformation to other reference systems (such as possible future updates of the potential model for Mars). The map projection is Sinusoidal for latitudes between $\pm 85^\circ$ and Polar-Stereographic for polar areas.

Adjustment of orientation data and the systematic derivation of HRSC high-resolution Level-4 data products apply to all HRSC stereo imaging sequences, except limb observations and Phobos and Deimos observations. Processing is performed orbit by orbit, beginning from the first orbits. The data products are supplied periodically to PSA and PDS and are made available to the public through these archives after their validation.

The formats and labeling of the HRSC data available through these websites (see Section 2) comply with PDS standards. Specific keywords related to the vertical datum and to the numeric representation of heights that are used for the DTMs are currently under review by PDS and are therefore listed as “MEX-specific” keywords in the PDS DTM label.

Fig. 2 shows an example of a HRSC Level-4 dataset, a combined representation of DTM and color orthoimages for one imaging sequence in a perspective view of Valles Marineris.

4. Approach for systematic derivation of data products

The MEX HRSC experiment has provided a large amount of stereo data on single orbital passes. The conditions under which these data have been acquired cause a variation of image quality and of the accuracy of the a priori orbit and pointing data (Jaumann et al., 2007; Gwinner et al., 2009). The systematic derivation of HRSC high-resolution Level-4 data

products for the entire dataset, with high internal consistency and with high absolute accuracy with respect to global reference data (MOLA) has to accomplish two core issues of data analysis.

For one, a central pre-requisite is an operational photogrammetric processing system that allows for the systematic, robust, and accurate reconstruction of the orientation data for each orbit, irrespective of variable conditions. In Section 4.1, we report on the conception and implementation of the procedure applied for the adjustment of MEX HRSC data.

The second core issue is a reliable procedure for 3D surface reconstruction at high resolution. It directly leads to the generation of the DTM which in turn forms the basis for the calculation of orthoimages. The methodology and procedures for the derivation of high-resolution DTMs from HRSC data by the experiment team have been described and analyzed in detail in Gwinner et al. (2009) and will be briefly summarized in Section 4.2.

4.1. Improvement of orbit and pointing data

The procedure for adjustment of MEX HRSC orientation data in the framework of systematic Level-4 processing is built on comprehensive experience gained on the improvement of orientation data for airborne HRSC imagery and other airborne multi-line sensors (Scholten et al., 2002; Scholten and Gwinner, 2004) and on extensive previous results of multi-line bundle adjustment of MEX HRSC data (Heipke et al., 2004; Spiegel 2007a,b; Schmidt 2008). Since we have also integrated developments that have not been presented elsewhere, we will address this part in more detail.

Bundle adjustment is a technique for reconstructing the imaging geometry based on a set of tie-points that are used simultaneously in a least-squares adjustment. Tie-points are identical (homologous) points in the different stereo channels and are identified by automated image matching techniques for HRSC stereo processing (Schmidt, 2008).



Fig. 2. Example of a combined HRSC high-resolution data product. Perspective view of Valles Marineris, MEX orbit 2039, from HRSC DTM and orthoimage.

Within multi-line bundle adjustment (see Hofmann et al. 1984 and Müller 1991 for the original formulation; and Grün & Zhang 2003 and Spiegel, 2007a, for more recent work), the exterior orientation parameters are modeled as connected 3rd order polynomials based on so-called orientation images (points within the imaging sequence for which orientation parameters are determined). A Gauss–Markov model is then applied to minimize the sum of the squared residuals of the observations (tie-point coordinates, camera calibration, exterior orientation parameters etc.).

Developments for multi-line bundle adjustment of HRSC data based on this approach yielded a significant improvement of the nominal orientation for most orbits (Spiegel, 2007a). However, examination of the resulting orientation data sets indicated, that in some cases the time interval between successive orientation images was too long for modeling existing high-resolution angular orientation errors. As a consequence, observed angular deviations from nominal pointing with frequencies of 0.1–0.2 Hz and substantial amplitudes up to 10 times HRSC's instantaneous field of view (IFOV) could not be corrected. If such effects are not modeled, they induce inconsistencies between the stereo channels, which affects the subsequent modeling of 3D points and thus can degrade resulting DTMs or at least hinder the full exploitation of the available stereo information. Choosing a shorter time interval between orientation images within bundle adjustment has led to improvements, but is not available as an operational solution at present.

Therefore, an extended overall approach to the improvement of orientation data has been adopted, that includes 1) bundle adjustment results, 2) a new approach for the photogrammetric adjustment, which models all observed inconsistencies of the nominal orientation and minimizes lateral and vertical offsets between HRSC DTM products and the MOLA dataset, and 3) a standardized testing and evaluation procedure for selecting the most reliable optimization result. The central idea of the revised adjustment process is the exploitation of the enormous amount of redundant high-resolution stereo information, which HRSC provides by its 5 panchromatic channels for the entire image swaths. The goal is the precise correction of the orientation angles in steps of 1 Hz (5–10 times higher than the frequencies of the observed phenomena), and the minimization of lateral and vertical deviations from MOLA by these corrections and by shifting the MEX orbit.

The newly developed sequential photogrammetric adjustment procedure (in the following called SPA) combines global optimization techniques with knowledge-based analysis of residuals at multi-ray intersections in an automated process. It investigates the highly over-determined multi-stereo forward ray intersections for many 3D points in order to retrieve robust correction values for the related angular orientation parameters continuously over the entire time interval of data acquisition within an orbit. In addition, the MOLA DTM is used as reference in order to enforce a best absolute fit of the HRSC model, both, laterally and vertically. Lateral and vertical displacements of the HRSC surface model are derived with SPA by analyzing the statistics of HRSC deviations to the MOLA data set over the entire area. SPA is applied in the same way, i.e. without any case-specific adaptation, to both, available bundle adjustment results (Spiegel, 2007a,b; Schmidt et al, 2008), as well as nominal MEX HRSC orientation data based on nominal pointing and reconstructed orbit data. Fig. 3 provides a sketch of the SPA procedure.

Through a systematic analysis of specific quality figures obtained during the SPA procedure, the best solution among different adjustment results is selected as the final adjusted orientation data set. These quality measures refer to the internal accuracy as well as deviations from MOLA data. Both, quantitative criteria as well as qualitative criteria evaluated by visual inspection of parameter maps are applied. In particular, the selected orientation data should provide

- the best internal accuracy (smallest mean forward ray intersection error),

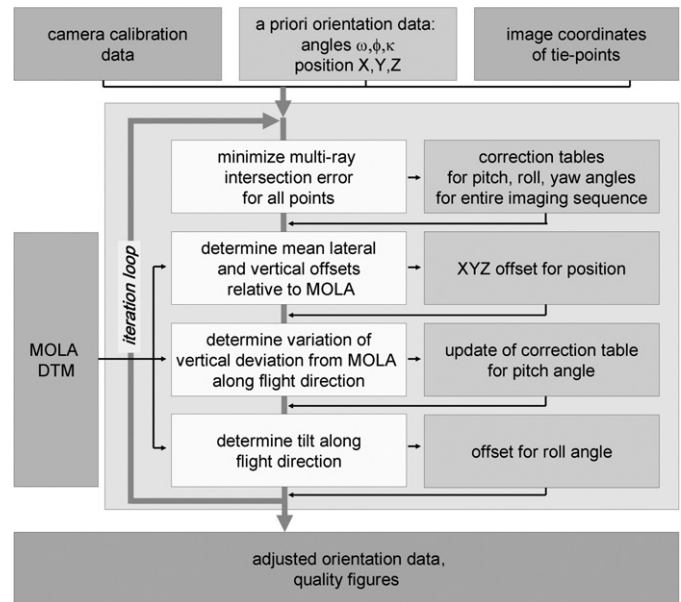


Fig. 3. SPA flow chart. Note that a priori orientation input data may represent nominal orientation or orientation already improved by bundle adjustment.

- the most homogeneous spatial distribution of accuracy (e.g. elimination of the effects of high-frequency variation of orientation angles), and
- the best fit to MOLA, including the smallest residual along-track variation of the vertical deviations from MOLA.

Orientation data consist of 3 components for position, X,Y,Z, i.e. the spacecraft/camera position in the Mars-fixed coordinate system x_m, y_m, z_m , and 3 angular pointing components that define the rotation matrix $\mathbf{R}_{m2c}(\phi, \omega, \kappa)$, i.e. rotations around the y_m, x_m, z_m -axes from the Mars-fixed coordinate system to the actual camera system x_c, y_c, z_c . These 6 components vary in time during the entire HRSC imaging sequence. Within SPA the rotation \mathbf{R}_{m2c} is typically split into two subsequent rotations. The first rotation $\mathbf{R}_{m2l}(\phi, \lambda)$ is a function of the local latitude and longitude and defines the rotation of the Mars-fixed coordinate system to a local tangential system x_l, y_l, z_l (with its axes co-aligned to the nominal spacecraft navigation and camera axis in the nadir-pointing case) at the respective epoch. The second rotation \mathbf{R}_{l2c} (pitch, roll, yaw) defines the rotation of the nominal local tangential system around its y_l, x_l, z_l -axis to the actual camera system. Camera calibration data (focal length and CCD positions in the focal plane) are also integrated in the SPA process, but in contrast to the orientation data they are used as fixed values.

An aspect of prime importance in the conception of SPA is a high number of tie-points. We aim at several hundred points for each second of the imaging duration (i.e. a few hundred thousand points for each entire orbit) in order to achieve high redundancy. Area-based multi-image matching is used for this task. Recall that SPA is fundamentally based upon this high redundancy, whereas the precision of each single point is fairly uncritical.

Each tie-point consists of up to 5 stereo observations (line/sample image coordinates of each stereo channel). In the first step of SPA, the forward ray intersection error of each point is used as the criterion for the optimization of orientation angles. SPA determines optimal correction values for the orientation angles by varying pitch, yaw, and finally roll for each tie-point. Recorded as a function of time, these values serve to construct correction tables for the orientation angles over the entire orbit. Subsequently, the distance of each imaging ray from the mean intersection point is investigated and additional corrections for the orientation angles are derived from across-track and along-track residuals.

Correction tables within SPA are quantized to 1 Hz. Hence, angular variations with frequencies lower than 0.5 Hz can be represented. It is not necessary to go beyond this value, since there has been no indication of higher frequencies for MEX's true orientation.

Fig. 4 provides an example of high-frequency variability of orientation angles within an orbit and their compensation in the different orientation versions.

Lateral deviations of the HRSC topography models, defined by the resulting object point clouds, are determined by a comparison of HRSC and MOLA raster DTMs. The HRSC model (gridded to 50/100 m) is shifted in sub-raster steps across the over-sampled MOLA data, registered to the same grid. Those along-track and across-track shifts yielding the smallest overall variance of the height differences at all grid points define the lateral correction values. The vertical offset correction value is the median of the final height differences (using the median, rather than the mean, minimizes the influence of bad points, e.g. caused by atmospheric dust). Lateral and vertical offsets are transformed to orbital shifts in the Mars-fixed XYZ coordinate frame. Residual local or regional trends within the height differences are further minimized by correction of the pitch angle for the respective stereo sensor observation times.

Finally, since for single image tracks the along-track stereo geometry does not allow for a robust detection of a general roll tilt of the entire HRSC model along the flight direction axis x_c without any ground reference, an analysis of the residual height differences to MOLA is used for the determination and correction of such tilts. Across-track shifts, which are implied by these tilt corrections, are compensated by the respective orbital shift.

Because each single optimization step changes the overall geometry and has an effect on the remaining parameters, SPA is an iterative process. The iteration stops, if within an iteration

- correction table updates improve the overall multi-ray intersection error by less than 1%, and
- lateral shifts are smaller than 25 m (half of the smallest HRSC DTM grid size), and
- the vertical offset and regional deviations to MOLA are smaller than 2 m, and
- the roll offset correction does not exceed the HRSC IFOV (0.0023°).

A typical example for the achieved improvement of internal consistency and absolute reference to MOLA is given in Fig. 5.

4.2. Derivation of digital terrain models

The derivation of HRSC high-resolution DTMs includes the generation of a dense set of accurate 3D points, and an interpolation technique that allows for the generation of a detailed continuous surface representation from these points, where variations in data density and precision are being taken into account. Previous experiments on generating high-resolution DTMs from HRSC data (Gwinner et al., 2009) and a systematic test in comparison with alternative approaches to HRSC stereo processing (Heipke et al., 2007) have shown that this process has to integrate adaptive processing components and efficient internal mechanisms for quality control in order to achieve optimal results. Due to the large data volumes involved, the procedure also has to work highly automatically. Since the methods and techniques applied for DTM generation within the systematic HRSC Level-4 processing are reported and analyzed in detail in Gwinner et al. (2009), we limit the description of the procedure to a short overview here. Subsequently, since they play an important role for the matching of HRSC stereo images, we briefly consider the effects of compression and image contrast on the 3D processing.

The generation of a dense set of homologous image points for the stereo images is based on sub-pixel multi-image matching using pyramid-based least-squares correlation after pre-processing by adaptive (variable bandwidth) Gaussian low pass filtering of the stereo images to reduce the effects of image compression and noise. Multi-image matching is organized as a two-stage process. We introduce an indirect epipolar constraint by reducing the search areas to the actually expected residual parallaxes in rectified stereo images. These are produced by ortho-rectification using an intermediate HRSC DTM with low resolution compared to the imagery.

Image matching typically results in datasets comprising 10^7 to 10^8 points for a single imaging sequence. Reconstruction of 3D coordinates for these points by least-squares forward intersection is followed by blunder elimination (using constraints on the number of stereo observations and thresholding of the intersection error), and

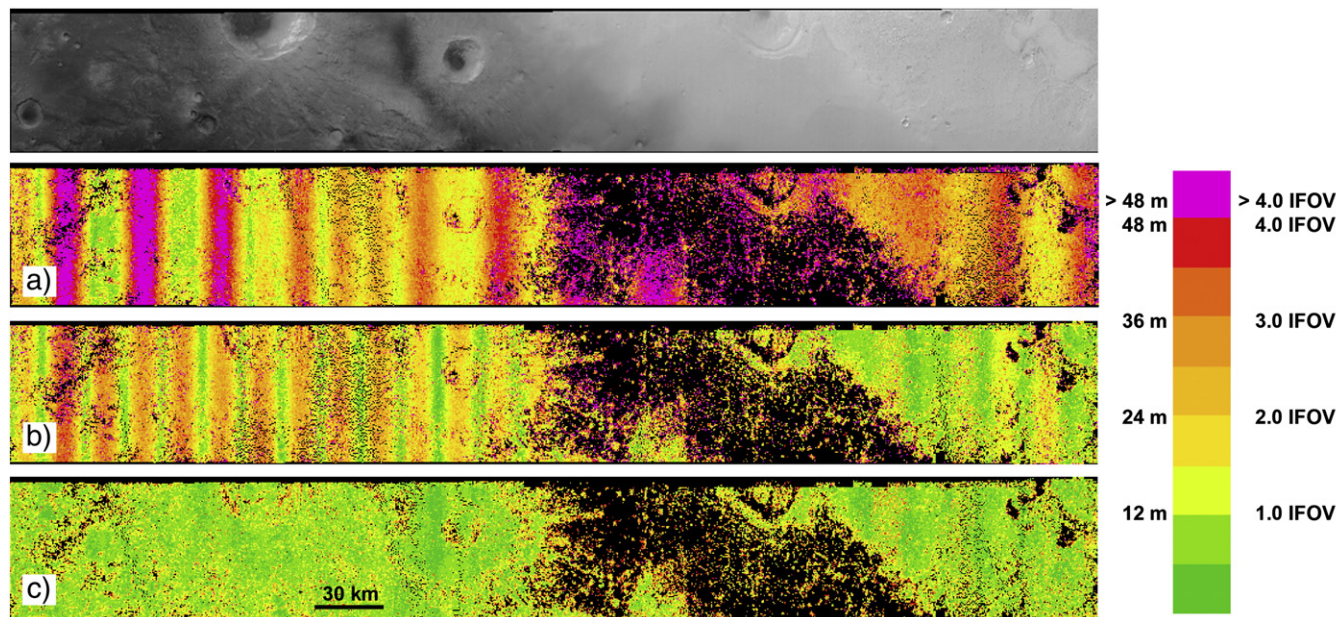


Fig. 4. Forward ray intersection error map, MEX orbit 2075, top: nadir image, flight direction from left to right. Intersection error in meters, and scaled to the HRSC IFOV resolution, a) using nominal orientation data, b) using bundle adjustment results, with time interval between successive orientation images being too long, c) using final SPA orientation results. Black areas: no points because of insufficient image contrast.

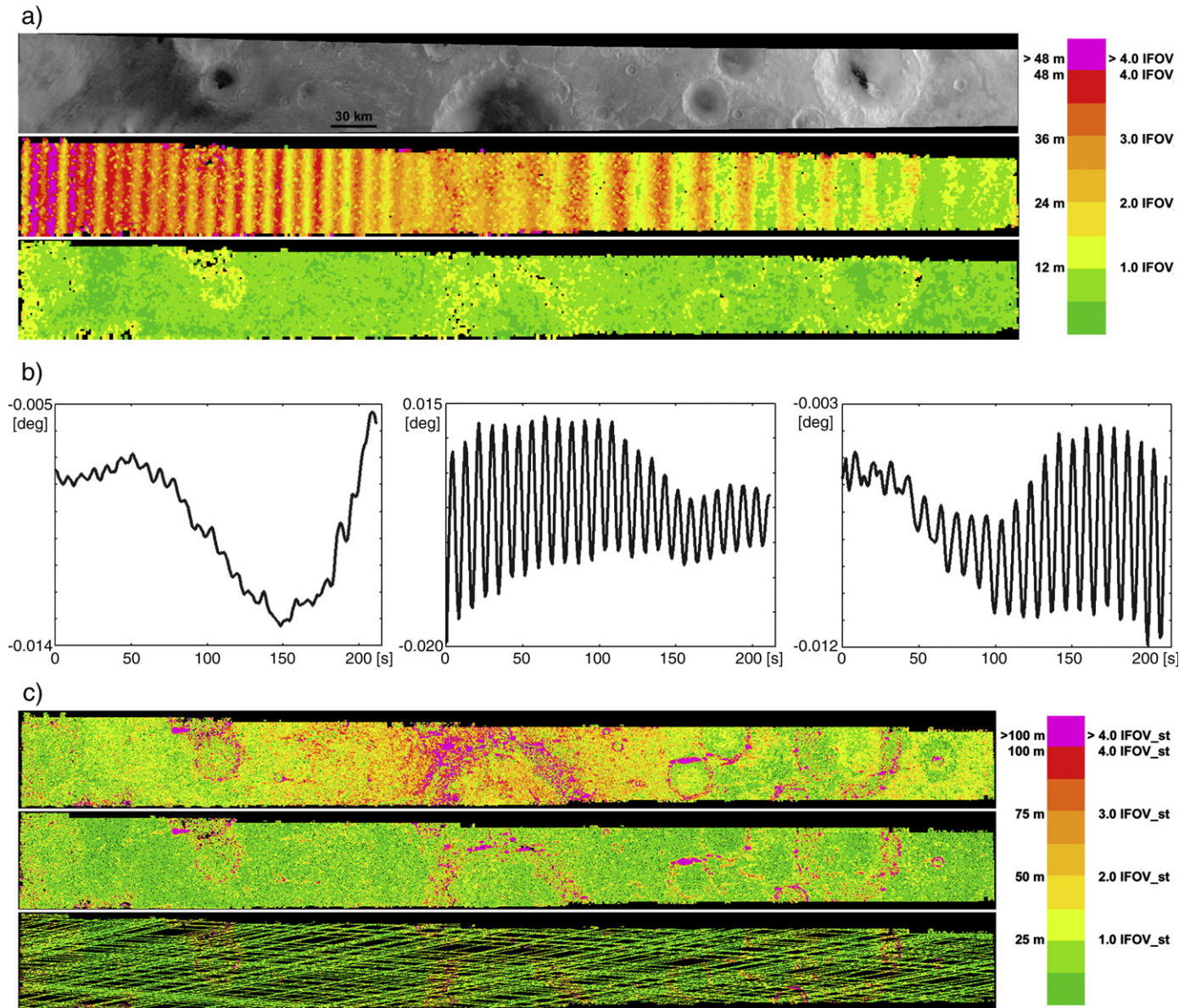


Fig. 5. a) MEX orbit #2258, flight direction from left to right. Top: nadir image, center: forward ray intersection error using nominal orientation, bottom: error using final SPA orientation results. b) SPA corrections of orientation angles pitch (left), roll (center), and yaw (right) over the complete imaging time interval of MEX orbit 2258. c) Large scale deviations of HRSC topography from MOLA, MEX orbit 2258, from interpolated MOLA raster. Top: using nominal orientation, center: using final SPA orientation results, bottom: deviations at MOLA tracks only. Deviations given in meters and scaled to the mean stereo resolution. Note that SPA results in the removal of wave-shaped, large scale offset variations and a laterally homogeneous minimization of vertical residuals.

finally by DTM grid interpolation (distance weighted averaging within a local interpolation radius). The overall process involves automatic procedures in combination with standardized quality checks.

The variable definition of the DTM grid spacing (Table 1) is motivated by the aim of an approximately constant density of 3D points entering a grid cell and a low percentage of data gaps closed by interpolation (grid filling rate), while the quality of the input data is variable in terms of mainly ground resolution and image contrast (quite often reduced due to atmospheric conditions met by HRSC on Mars; see Hoekzema et al., 2009–this issue). A general guideline for the selection of the grid spacing is the highest matching resolution applied successfully during parameter tests. However, within an interactive step, also the spatial distribution and quality of the obtained object points are evaluated and contribute to the final selection of the grid spacing.

Adaptive, space-variant filtering of HRSC stereo images (Gwinner et al., 2005, 2009) allows us to maintain the success rate of image

correlation close to the rate that could be expected for non-compressed data, as suggested by analysis of test images from Mars orbit that have not been compressed. For comparison purposes, another regular (i.e. compressed) imaging sequence acquired under very similar conditions exists (Fig. 6). The matching success rate obtained for the compressed data after adaptive filtering was reduced by 2% and 8%, for the two most frequently used matching resolutions, in comparison to the no-compression dataset. Conversely, compression was found to reduce the number of useful point determinations by as much as 40 and 30%, at the same resolutions, when no image filtering was applied to the compressed images. In addition, the deviation of resulting DTM heights from those of the no-compression case is reduced by adaptive filtering by about 10% (standard deviation of height difference 15.6 m and 13.9 m, respectively). From the standard deviation with MOLA DTM heights, the magnitude of the residual contribution of compression-related noise to the DTM after adaptive filtering can be estimated as few meters. This is a small

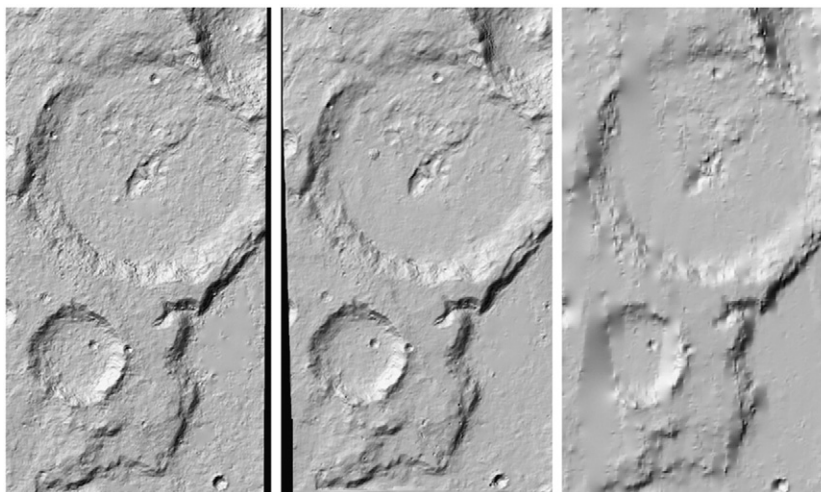


Fig. 6. Effect of image compression on the DTM results. Left: DTM from compressed data after adaptive filtering of the stereo images (MEX orbit 3047). Center: the same area using images without compression (MEX orbit 3036). Right: MOLA DTM for comparison. Note that the completeness of surface representation is nearly unaffected in the compression plus filtering case, while the noise on smooth surfaces (well represented in the MOLA DTM) is moderately increased.

fraction of the total deviation of the no-compression result from MOLA (standard deviation of 22.2 m without compression; 24.9 m for the case of compression and adaptive filtering; refer to Section 6 for typical deviation values to MOLA).

Finally, experiments with non-adaptive approaches to image filtering (i.e. applying fixed filter sizes) showed that these may degrade the accuracy and reliability of the image matching at high resolution significantly (Gwinner et al., 2009), because the constant filtering bandwidth does not properly account for the high variability of textural properties and compression features of HRSC imagery.

Image matching depends substantially on image contrast. For this reason, consideration has to be given to possible limitations of stereo processing by image contrast. Note that HRSC is an 8-bit camera, that compression also affects the radiometric resolution of the data, and that the contrast observed from Mars orbit is often strongly reduced by the atmosphere. Fig. 7 presents the mean intersection error that was achieved within the stereo analysis of each of more than 200 imaging sequences of the nominal mission that allowed for deriving high-resolution DTMs, as a function of the mean image contrast of the respective stereo images. Contrast is defined here as the dynamic range per image line, measured in digital numbers (DN), and averaged

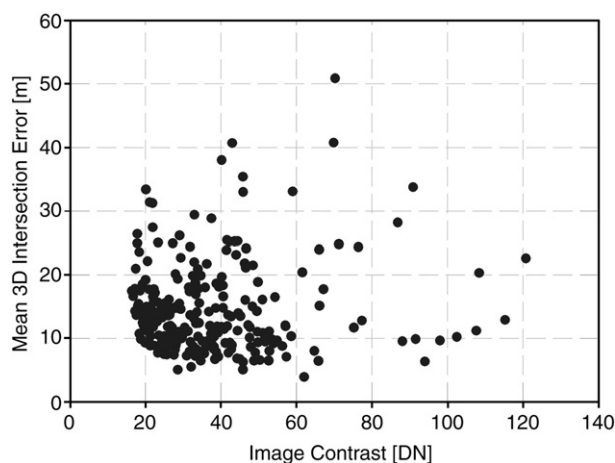


Fig. 7. Contrast as a limiting factor for point precision. Mean intersection error, derived for each of more than 200 stereo datasets of the nominal mission that have yielded high-resolution DTMs, is plotted vs. the mean image contrast of the respective dataset. Note that precision appears to be independent of contrast for values >30 DN, and sub-pixel precision is principally possible for all observed contrast values.

over all image lines of the respective stereo images. Fig. 7 shows that sub-pixel accuracy can be achieved for the full range of image contrasts that are encountered (see Fig. 2 for comparison with the range of stereo ground resolutions). A sharp lower boundary delimiting the distribution of the data points is present for contrast values of about 30 DN and smaller, but not for contrast values greater than 30 DN. This suggests that only for a sub-set of image data belonging to this contrast range <30 DN, the contrast was the decisive limiting factor for further improvement of sub-pixel accuracy during the matching process. From this and from the absence of a general correlation between contrast and precision, we can infer that no significant contrast-related limitation of 3D precision is present, at least for contrast values larger than about 30 DN, which is a value that is achieved by a large percentage of the datasets.

4.3. Orthoimages

HRSC orthoimages are high-level topographic data products obtained by rectification of the images based on the high-resolution DTMs (see Scholten et al., 2005, for more information on this differential rectification process). For this reason, Level-4 HRSC orthoimages are available exclusively for areas covered by HRSC high-resolution DTMs. Orthoimages provide the metric properties of a map and complement the continuous description of surface topography represented in the DTM. The horizontal resolution of the orthoimages (Table 1) is directly linked to the best ground resolution within the original image. The rectification process makes use of the same improved orientation data as the DTM processing and therefore the orthoimages are co-registered to MOLA in the same way. The only additional pre-processing step for orthoimages with respect to the calibrated Level-2 image consists of a histogram-based linear contrast stretch. This does not affect the linear metrics of the radiometric calibration, and is applied independently for each image channel.

The improvement of horizontal position accuracy of the Level-4 orthoimage as compared to the Level-3 image data product (which is rectified using the MOLA 463 m DTM instead of the high-resolution HRSC DTM) is illustrated in Fig. 8. For this purpose, the Level-3 image was recalculated using the improved orientation data obtained during the systematic Level-4 processing. Since the radiometric pre-processing and the orientation data applied, therefore, are identical for both datasets, the larger color differences visible in Fig. 8 that occur prevalently in areas with strong topographic relief can be directly related to color seams in the Level-3 image. These are caused by the less detailed height information provided by the MOLA data used for

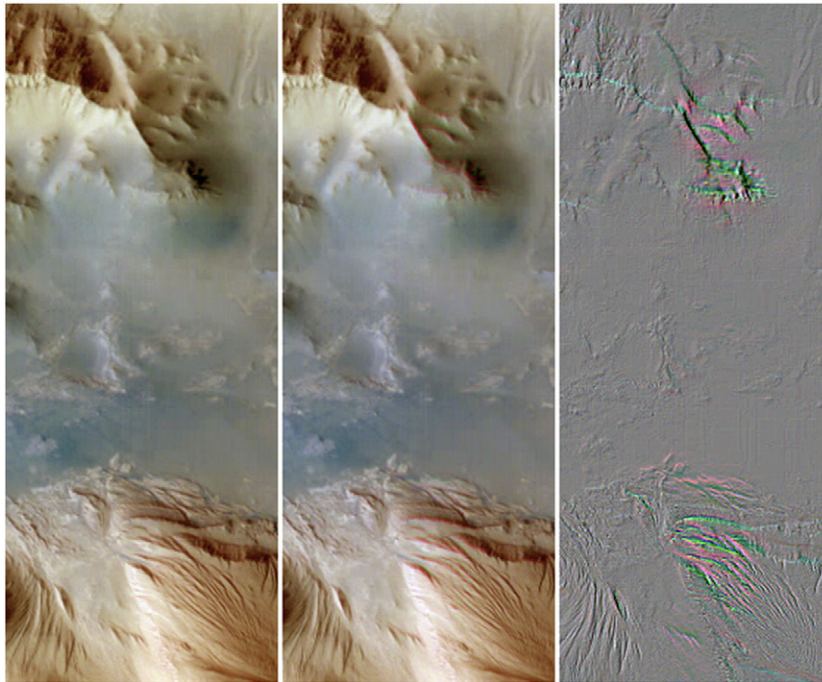


Fig. 8. MEX orbit 2039, Valles Marineris. Left: HRSC Level-4 red-green-blue orthoimage. Center: corresponding HRSC Level-3 orthoimage, based on MOLA DTM, and showing color seams in steep terrain that result from less detailed height information. Right: difference image of the Level-3 and Level-4 images.

the Level-3 processing, which, due to the different observation geometries among the color channels, leads to horizontal displacements on the order of the pixel size.

5. Overall performance characteristics

5.1. Adjustment of orientation data

The datasets considered in the following sections comprise stereo imaging sequences for which the processing has been finished before December 2008, i.e. orbit numbers before MEX orbit 2217. The total number of HRSC stereo imaging sequences for Mars (excluding limb observations) up to MEX orbit 2217 is 737. The results of orientation adjustment by SPA for these datasets can be grouped as follows:

Total number of orbits with SPA results	676 (92%)
– using initial values based on nominal orientation:	264 (39%)
– using initial values based on bundle adjustment:	365 (54%)
– using bundle adjustment results as they are:	47 (7%)
Total number of sequences without any SPA results:	61 (8%)

Failures to derive SPA results are mainly caused by image degradation (e.g. atmospheric dust, strong image compression, image gaps, etc). The total number of available bundle adjustment results for the same orbit range is 544 (or 74% of all datasets).

Fig. 9 displays the overall improvement of the forward ray intersection error by SPA. On average, SPA increases the internal geometric consistency within an orbit by about 34% to pixel or sub-pixel accuracy. The mean forward ray intersection error could be reduced from 2.47 to 1.64 nadir pixels, or 1.13 to 0.74 mean stereo pixels. The mean ground resolution of the nadir channel of all processed orbits is 20 m/pixel, the mean stereo resolution is 43 m/pixel. Note, that these statistics for the internal accuracy, as well as the vertical residuals to MOLA stated below (**Fig. 11**), have been derived from SPA points. As pointed out earlier, these points do not fully exploit HRSC's stereo processing potential based on additional processing steps as described in **Section 4.2**. Therefore, accuracy statistics will be considered further in the context of the final high-resolution DTM processing (**Section 5.2**).

A further criterion for the success of the SPA process is the orbit-wise referencing to the global MOLA data set by the correction of lateral and vertical displacements of the resulting HRSC topography models. **Fig. 10** illustrates the magnitudes of the corrections for all datasets. For about 90% of the orbits the corrections are smaller than 200 m along-track, 200 m across-track, and up to 100 m vertically. Other orbits require greater corrections, up to or even more than 1 km, in particular after safe-mode conditions and when the MEX spacecraft is near eclipses. In these cases, tracking of the spacecraft signal is impossible or can only provide degraded orbit data as initial information.

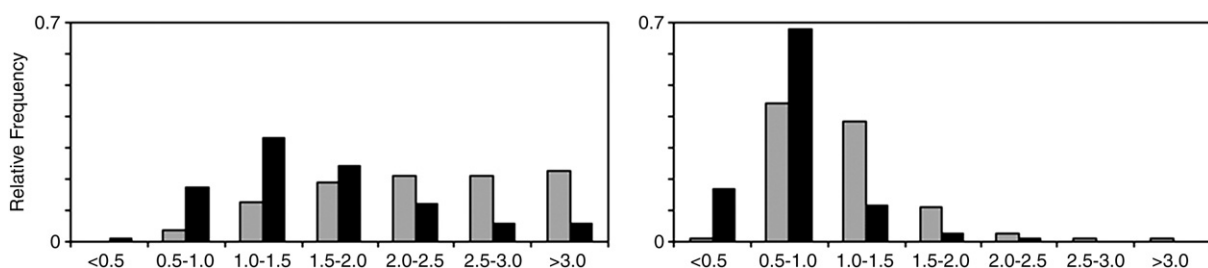


Fig. 9. Forward ray intersection error of all mapping orbits optimized by SPA, using nominal orientation (gray) and SPA results (black). Error scaled to mean nadir resolution (left) as well as to the mean stereo resolution (right) of the respective imaging sequences.

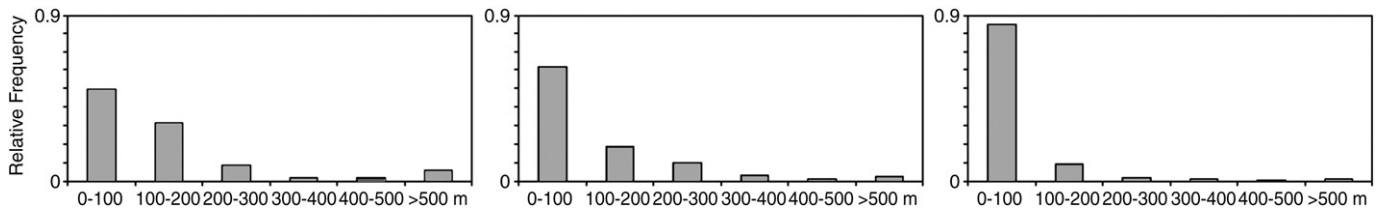


Fig. 10. Distribution of along-track (left), across-track (center), and vertical (right) corrections by SPA.

The quality of all optimized HRSC data sets with respect to the achieved vertical fit to MOLA is shown in Fig. 11. Note that all residuals are generally the result of HRSC and MOLA height uncertainties as well as – compared to HRSC – MOLA's low lateral resolution. These points will be further investigated based on the high-resolution DTM product (Section 6).

The left part of Fig. 11 shows that, using all SPA points, the nominal MEX orientation constitutes a broad peak of residual vertical offsets to MOLA, centered at about 12 m. The standard deviation is 140 m. With SPA optimization the curve is well centered around zero, and the absolute values of vertical differences have also decreased significantly. The residuals over all points now show a standard deviation of 87 m. In the right part of Fig. 11, we consider the mean vertical residuals of each individual imaging sequence separately. The standard deviation of 1.9 m suggests that the accuracy of the vertical fit to MOLA can be expected to be better than 4 m, i.e. approximately 10% of the mean stereo resolution, for almost all of the MEX HRSC orbits.

A final test of the lateral adjustment to MOLA is performed for each imaging sequence on the basis of the final HRSC high-resolution DTM. The residual shifts determined for all datasets during these tests show a standard deviation of 0.53 HRSC grid cells for both line and sample direction. Accordingly, the lateral deviations from MOLA can be expected to be smaller than the grid spacing of the respective HRSC DTM in most cases and smaller than 1.5 grid cells for almost all datasets. In length units, we obtain a standard deviation of 62 m for the line direction and 56 m for the sample direction (see also histograms Fig. 12). Thus, the horizontal uncertainty amounts to a fraction of the MOLA grid size. A value smaller than 100 m can be expected for most HRSC DTMs. Note that these values are on the order of the estimated horizontal uncertainty of the MOLA data product itself (<100 m; Neumann et al., 2003). It is also important to note that these residual offsets represent the uncertainty of position in terms of a rigid translation of the entire HRSC models with respect to an external reference (MOLA). They have to be distinguished from the internal lateral precision of the HRSC model, which corresponds to the precision of the HRSC 3D points and is more accurate in general.

5.2. DTMs and orthoimages

The statistics presented in Table 2 report on relevant quality parameters related to 3D accuracy, spatial resolution, and coverage, as

they have been achieved for the entire product dataset. For the sake of completeness, also the statistics related to orthoimage resolution are reported, although they, by definition, directly reflect the ground resolutions of the respective raw images.

Recall that the constitutive requirements for the generation of raster DTM at a given resolution are related to an appropriate density and precision of the available 3D points. A measure for HRSC point precision is provided by the 3D error derived from the quality of multi-ray forward intersection. The average 3D intersection error calculated from the mean values of all datasets is 12.9 m (Table 2). About 40% of the DTMs have a mean intersection error of better than 10 m, and about 95% of better than 25 m. Note that lower point precision generally has to be compensated by increasing the extent of local filtering operations during DTM interpolation and thus by a reduction of effective spatial resolution.

The geometric interpretation of the 3D intersection error is the length of a vector defined by the precision values related to each of the three coordinates of a global Cartesian reference system. The 3D error can therefore be interpreted as an upper limit for the relative error of each of the local north, south and height position components. Furthermore, results of bundle block adjustment have shown that the vertical error component is about 0.9 times the 3D error, and the 2D planimetric (x,y) error component is about 0.43 times the 3D error for HRSC (Schmidt et al., 2005). Accordingly, the average 3D error obtained from all datasets (12.9 m, Table 2) can be translated to a mean height error of 11.6 m and a mean planimetric error of 5.5 m.

The mean 3D intersection error can also serve as an estimate for the planimetric precision of the orthoimages. Taking into account that up to 5 stereo observations contribute to a 3D point, and thus to its error, and using again the relationship between planimetric and total 3D error from Schmidt et al. (2005), the mean planimetric precision for a single stereo sensor is about 95% of the 3D error. Therefore, and because the mean off-nadir angle of the sensors used for orthorectification (near-infrared, red, green, blue, panchromatic nadir; 6.4°) is smaller than the mean off-nadir angle of the five stereo sensors used for point determination (12.7°), the 3D error represents also a reliable upper limit for the planimetric precision of HRSC orthoimages. This means that the sub-pixel precision achieved with respect to the stereo images can be applied also for the Level-4 orthoimages. Note, however, that significant local DTM errors can lead to local distortions of orthoimages, as exemplified by color seams in the Level-3 image presented in Fig. 8.

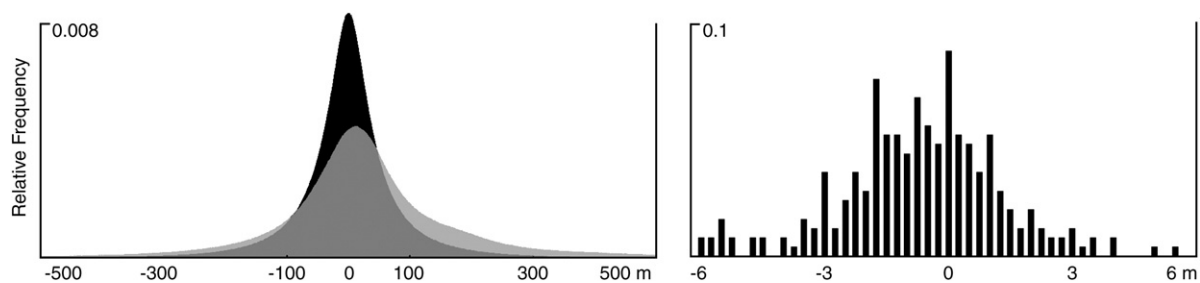


Fig. 11. Statistics for vertical adjustment to MOLA. Left: distribution of vertical residuals to MOLA of all HRSC SPA points at MOLA tracks only, before (gray) and after (black) optimization. Right: distribution of mean vertical residuals of single orbits after optimization.

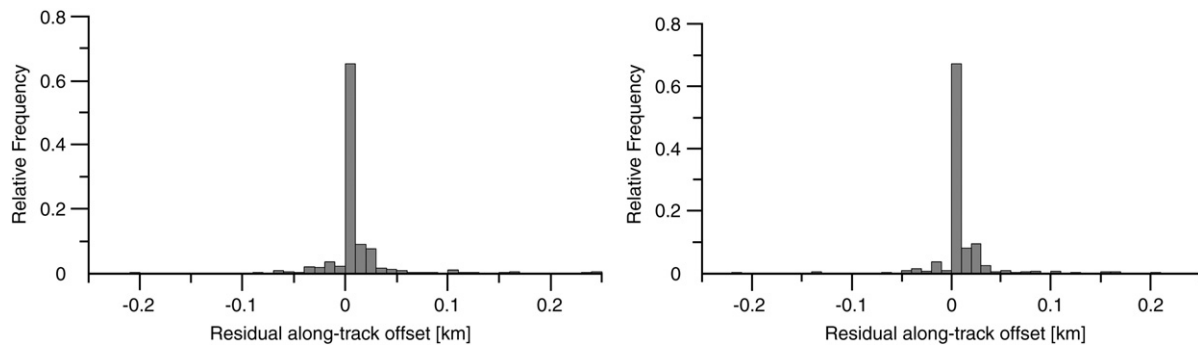


Fig. 12. Quality of lateral adjustment to MOLA. Distribution of residual shift estimates in kilometers for along-track (left) and cross-track (right) direction.

Concerning the general limitation of DTM resolution by point density, we note from Table 2 that the average number of 3D points that fall into one raster cell of the DTM grid is larger than 1.5 for almost all datasets (about 5 ± 3 points, on average). Moreover, the grid filling rates (i.e. the fraction of grid cells that actually contain measured 3D points) obtained for all DTM datasets are in line with previous results based on a smaller dataset (Gwinner et al., 2009) and show acceptable minimum values for those DTMs that had to be generated from comparatively less dense 3D point sets. About 85% of the datasets have a filling rate of better than 0.5, and 5% of better than 0.94. These numbers support the appropriateness of the chosen grid spacing values (and its variation).

Note that, although Gwinner et al. (2009) have demonstrated that the lateral point coverage is improved significantly by applying adaptive processing techniques, the occurrence of matching gaps cannot be completely avoided (see also Kirk et al., 2006; Heipke et al., 2007). Image inspection and comparison with the MOLA DTM suggest that the gaps are typically related to environmental conditions and to a small number of specific surface types (see Section 6).

Since the above mentioned requirements of sufficient point density and precision principally tend towards a reduction of DTM resolution in favor of increased reliability and coverage, it is of interest to consider to what extent the concurrent aim of a detailed terrain representation at maximum possible resolution is achieved. Fig. 13 contrasts the actually adopted grid spacing for each DTM with the respective ground resolution, point precision, and point density per surface area.

The grid spacing is seen to follow clear trends towards smaller grid spacing for each of these parameters, i.e. for higher ground resolution, lower intersection error, and higher point density. The scatter of the values is a consequence of the concurrent impact of a number of different parameters. As rules-of-thumb, the DTM grid spacing reflects about two times the mean stereo ground resolution and 7 times the intersection error.

It is also instructive to consider the limiting cases apparent from Fig. 13. The upper boundary for the DTM grid size is quite well defined

with respect to the mean stereo resolution (factor of about 3), whereas the lower boundary of the DTM grid spacing is marked by a minimum number of points per surface area of approximately 1 point per grid cell (e.g. 100 pts/km² is the lowest point density that was used to generate a DTM with 100 m grid spacing). Conversely, the lower boundary of the DTM grid spacing is not well defined with respect to the mean stereo resolution. This is expected because of the occurrence of exceptionally high sub-pixel accuracy (0.1–0.2 mean stereo pixels) under specific conditions (e.g. very clear atmosphere, low resolution image sequences with very good contrast and orientation data, etc.). Finally, we note that in almost all cases the chosen grid spacing is more than 3 times larger than the intersection errors. This provides adequate safety against the occurrence of misregistered 3D points and complies with common practice in Earth remote sensing. On the other hand, the average factor of about 7 between intersection error and grid spacing is quite high and indicates that HRSC DTM generation for Mars is mainly limited by point density, not point accuracy.

Nevertheless, with a number of 1.5 million to 250 million 3D points for each dataset, also the point density can be considered to achieve a high standard. All DTMs reported here are based on a total of more than 18 billion points. Relative to the planet surface, the average point number per DTM dataset is 723 pts/km² (i.e. one point every 37 m) with a 90% range of between 75 pts/km² and 1925 pts/km², where lower values correspond to DTMs that have a larger grid spacing (Fig. 13). Note, however, that the horizontal distribution of these points can show density variations caused by the dependency of stereo image matching on image texture.

By December 2008, high-resolution Level-4 data products for 549 imaging sequences have been completed. They cover a surface of about 30 million km². For part of the remaining additional imaging sequences with valid SPA results, high-resolution processing was unsuccessful because of insufficient surface visibility due to atmospheric phenomena (clouds, dust, haze) or because of significant data losses producing image gaps. For another part, high-resolution processing is currently not finished.

Table 2

Average values and variation of the main quality parameters for the data products of the nominal mission.

	Average	Standard deviation	5th percentile	95th percentile
Mean intersection error [m]	12.9	6.3	6.2	25.1
Sub-pixel accuracy [] (relative to mean nadir resol.)	0.67	0.23	0.36	1.10
Sub-pixel accuracy [] (relative to mean stereo resol.)	0.30	0.11	0.16	0.53
DTM 3D point density [points/grid cell]	4.5	3.2	1.5	9.5
DTM 3D point density [points/km ²]	723	688	75	1925
DTM grid filling rate []	0.70	0.16	0.41	0.94
DTM grid spacing [m]	93.1	37.6	50	175
Orthoimage resolution (panchromatic) [m]	16.9	9.7	12.5	50
Orthoimage resolution (color) [m]	80.8	38.9	50	100

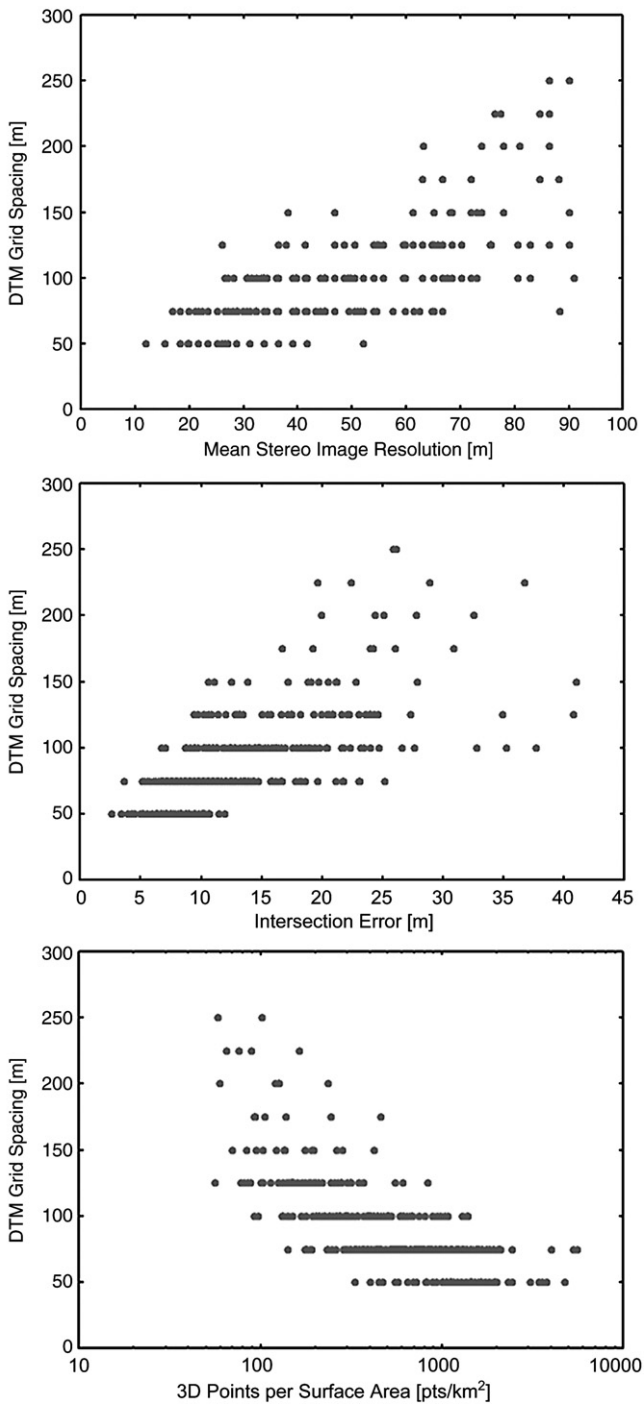


Fig. 13. Achieved DTM grid spacing as a function of ground resolution, intersection error, and point density.

6. Comparison between HRSC high-resolution DTM and MOLA

After accurate adjustment of the HRSC model to MOLA, the remaining deviation of height values between the two dataset can be ascribed to measurement uncertainty on both sides as well as systematic differences in the representation of topographic detail. Comparison of both DTMs offers the possibility to assess additional quality aspects of HRSC DTMs. Moreover, it is of interest to investigate the complementarities and the specific strengths of the two datasets – in view of the topography of Mars and as representatives of their instrument types. Similarly, future comparison with DTM datasets

derived from Mars Global Surveyor and HiRISE data, which were not available for the work presented in this paper, will be of interest.

Table 3 shows 1) the presence of considerable height differences between the MOLA and HRSC DTM datasets in terms of standard deviation and mean absolute value, and 2) the significant reduction of the standard deviation of the differences when data gaps filled by interpolation (in both datasets) are excluded.

Following Heipke et al. (2007), the deviation of heights along MOLA measurement tracks can be interpreted as an error measure for HRSC DTMs. By this, we find a mean uncertainty of height in terms of standard deviation of 39.7 m over all HRSC DTM products, with a spread (standard deviation) of 26.5 m among the different HRSC datasets, and with a range of about 16.2 m to 81.2 m (Table 3). Excluding data gaps from the analysis also for the case of the HRSC DTM leads to a general reduction of the deviation, e.g. an average standard deviation of 34.5 m. Both values are about twice as high as would be expected from the internal estimates of the height error of the two datasets (both about 10 m), a discrepancy that has been also observed by comparison of height profiles derived from MOLA and HRSC (Gwinner et al., 2009). In difference maps, larger height differences are often associated with prominent relief features (Fig. 14, right side), suggesting that there are in fact systematic differences in resolving relief elements characterized by high terrain curvature. Sampling effects due to the considerable difference in spatial resolution between the two data sets might explain this discrepancy. The distance between single MOLA shots is 300 m along-track, the nominal spot diameter is 168 m. Testing this hypothesis would have to rely on suitable external high-resolution DTM.

Table 3 and Fig. 15 indicate evident differences between HRSC and MOLA with respect to the interpolation of gap areas. Measurement gaps, i.e. gaps in the lateral coverage of the surface by height measurements, are present for both datasets. They reflect the completeness of the surface reconstruction by the specific technique.

Relative to the case where all measurement gaps are excluded (i.e. masked out) during the determination of height differences, the height deviation increases by about 15%, when interpolation areas of HRSC (but not MOLA) are included. In the opposite case, when interpolation areas of MOLA (but not HRSC) are included, there is a larger increase by about 40%, and the values approach the case where interpolation areas are included in the analysis on both sides. The local presence of large height differences between MOLA and HRSC, which occur in elongated areas aligned with the measurement tracks of MOLA, has been described elsewhere (Heipke et al., 2007; Gwinner et al., 2009; see also Fig. 14).

The increased deviation related to MOLA gaps depends on latitude (Fig. 15). It continuously increases from the poles (where MOLA tracks show very dense spacing) towards the equator. For latitudes within $\pm 20^\circ$, the deviation is almost doubled due to the frequent occurrence of large MOLA gaps.

Table 3

Height difference MOLA–HRSC, and its dependency on interpolated measurement gaps.

Measure of deviation	Standard deviation	Mean absolute value of difference
Average, 5th and 95th percentiles		
Height differences MOLA tracks vs. HRSC DTM (without gaps filling by interpolation) [m]	34.5	24.1
Height differences MOLA tracks vs. HRSC DTM [m]	16.2/58.7	11.2/43.7
Height differences MOLA DTM vs. HRSC DTM (without gaps filling by interpolation) [m]	39.7	24.9
Height differences MOLA DTM vs. HRSC DTM [m]	16.2/81.2	11.2/48.7
Height differences MOLA DTM vs. HRSC DTM [m]	48.3	29.9
Height differences MOLA DTM vs. HRSC DTM [m]	20.7/91.2	13.7/56.2
Height differences MOLA DTM vs. HRSC DTM [m]	49.9	29.2
Height differences MOLA DTM vs. HRSC DTM [m]	21.2/93.7	13.7/53.7

First numbers are average values for all datasets, followed by respective minimum and maximum values (5th and 95th percentiles). “Track-to-no gaps fill” case: differences at MOLA measurement tracks only, and excluding HRSC data gaps. “Grid-to-no gaps fill case”: differences between both DTM, excluding HRSC data gaps. “Track-to-grid” case: differences at MOLA measurement tracks only, without excluding HRSC data gaps filled by interpolation. “Grid-to-grid” case: differences of the DTM without excluding any data gaps.

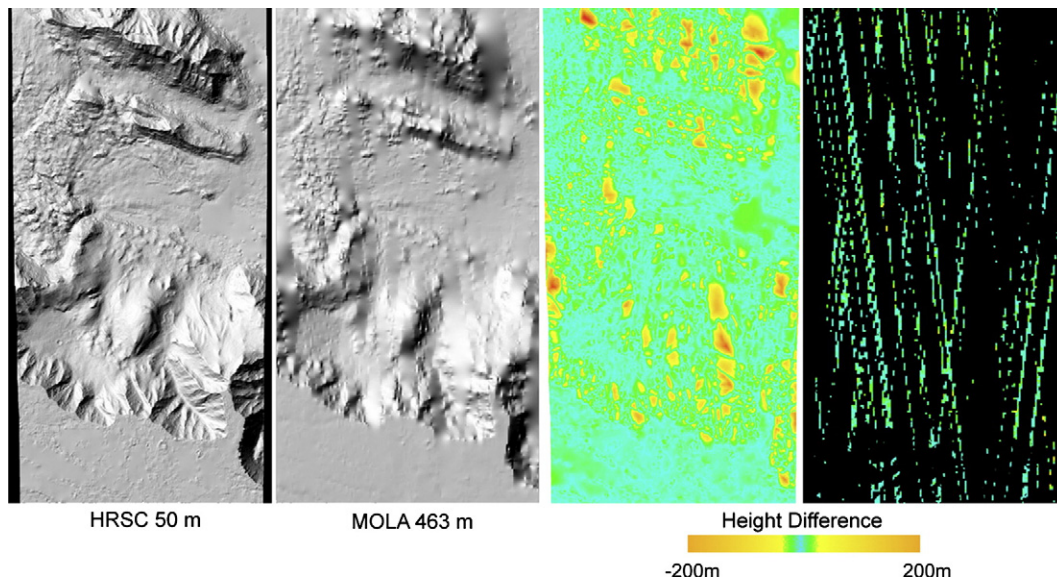


Fig. 14. Difference maps between MOLA and HRSC DTMs, with and without excluding data gaps. Left side: shaded relief maps for comparison. Note that the persisting height deviation observed when measurement gaps on both sides are excluded can be often associated with prominent relief elements such as narrow valleys and ridges, etc. Ophir Labes, Valles Marineris, south is up.

Conversely, the deviation that can be related to interpolated areas in HRSC is smaller and does not follow any apparent latitude dependency. This allows us to conclude that interpolation areas have a comparatively small impact on the quality of HRSC DTMs, although these in fact contain a not negligible fraction of such areas (see Section 5.2).

The low interpolation errors observed for the HRSC DTMs suggest that a) typical gap areas, by their nature, are smooth enough to allow for low interpolation errors, which in fact frequently accords with visual inspection, and that b) the immediate vicinity of the gaps is usually well represented in the DTM by accurate height values, which

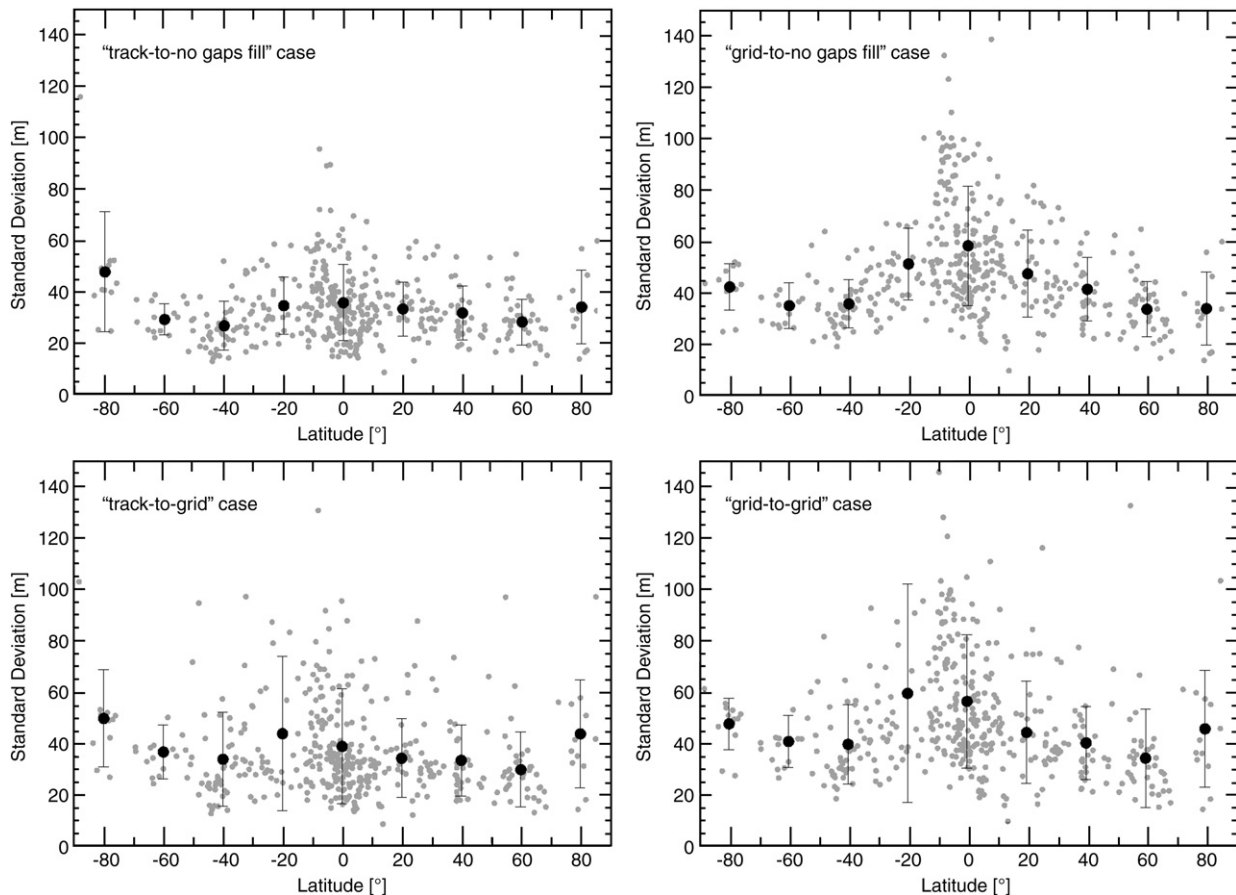


Fig. 15. Standard deviation of height difference MOLA–HRSC vs. latitude of the center of the HRSC DTM. “Track-to-no gaps fill” case: differences at MOLA measurement tracks only, and excluding HRSC data gaps. “Grid-to-no gaps fill” case: differences between both DTM, excluding HRSC data gaps. “Track-to-grid” case: differences at MOLA measurement tracks only, without excluding HRSC data gaps. “Grid-to-grid” case: differences of the DTM without excluding any data gaps.

allows for well-constrained interpolation. The results also suggest that height profiles (i.e. cross sections) that do not follow MOLA tracks should usually be more reliable when extracted from HRSC DTM, except for high latitude areas (latitudes beyond about $\pm 70^\circ$).

Comparison with MOLA for many datasets suggests that there are mainly just two surface types that frequently show poor image texture causing failures of matching HRSC images from Mars orbit: level (or very smoothly undulated), dust covered terrain, and bare ice surfaces. On the contrary, many of the examples of HRSC DTM gaps are found to be related (or also related), to particular environmental conditions, in particular to local atmospheric phenomena (clouds, dust, strong haze), solar elevation angles close to 90° , or deep cast shadows (met quite rarely, however, because of the scattering properties of the atmosphere of Mars). In contrast, the observation gaps in the MOLA dataset are primarily related to the orbit tracks and are thus of a more systematic nature.

7. Summary and conclusions

In this paper we have reported on the achievements of the HRSC experiment onboard Mars Express relative to one of its major aims, the mapping of the topography of Mars by high-resolution DTMs and orthoimages. A mapping program for the exploitation of the complete HRSC dataset has been initiated, and has allowed by now to provide high-resolution products for most of the datasets acquired in the nominal mission.

Adjusted orientation data are derived from a priori camera position and pointing within a specifically designed photogrammetric optimization process for each HRSC imaging sequence. A priori information can consist of nominal orientation and reconstructed orbit data, or of results from bundle adjustment. Pointing information is continuously optimized so that the multi-ray intersection error over the entire imaging sequence is minimized and a consistent 3D model is achieved. Applying the techniques for image filtering, point determination at high resolution and for quality control involved in the DTM processing, a mean precision of the resulting 3D points better than the mean resolution of the stereo images was achieved for all product datasets. On average, we obtain a sub-pixel precision of 30% of the mean stereo image resolution. 90% of the datasets are within the range 15 to 50% of the mean stereo image resolution. This corresponds to an average intersection error of 12.6 m, where 95% of the datasets yield values better than 25 m, and 5% of the imaging sequences provide mean intersection errors of better than 6 m.

While the intersection error provides a measure for the internal consistency of the HRSC models, the absolute accuracy of their registration in global coordinates is related to the quality of the adjustment to MOLA data. Absolute referencing of the HRSC models by adjustment to MOLA data is achieved by lateral and vertical offset corrections of the orbit position parameters, as well as by eliminating across-track tilt angle biases. The horizontal co-registration with MOLA is typically better than 100 m for most HRSC DTMs. This is a fraction of the highest resolution MOLA grid size. Vertical offsets are reduced to less than 4 m for almost all orbits. The applied sequential photogrammetric adjustment procedure (SPA) succeeds to detect, model and correct for high-frequency angular variations of the platform attitude based on the stereo pushbroom imagery.

The generation of high-resolution DTM from HRSC data, which has been the subject of extensive experimental studies during the recent years, yields results that are in line with the characteristics expected from the previous results, and partly surpass these. HRSC high-resolution DTMs are typically generated at a grid size of 2 times the mean ground resolution of the stereo images (up to 50 m DTM grid spacing). The grid size is usually not larger than 3 times the mean ground resolution of the images. The DTM grid spacing is also generally more than 3 times larger than the precision of the integrated 3D points (reported above), which provides high safety against misregistration of

height values. Statistically, every grid cell of a HRSC DTM is based on at least one measured 3D point. Specific tests have also shown that the precision of the 3D points is only marginally limited by the available image contrast of HRSC images (compressed 8-bit data). Moreover, the major effects of compression can be effectively compensated by appropriate adaptive processing techniques.

Comparing DTMs obtained from laser altimetry data and from stereo camera data, we conclude that the specific strengths of the two approaches complement each other distinctively, which confirms the current trend to include both instrument types on planetary exploration missions. While HRSC stereo images allow for a more detailed terrain reconstruction that is degraded by interpolation artifacts on measurement gaps to a surprisingly low degree (contribution of about 15% to the overall height uncertainty), altimetry profiles provide a straightforward means to obtain global shape parameters that can serve as a basis for co-registering other data and deriving global reference systems. Since on Mars morphological features typically contribute much stronger to the visible surface diversity in the panchromatic spectral range of HRSC than albedo variations that are not connected to morphological changes, we note also a duality related to relief strength, where HRSC DTM usually provides a more accurate representation of areas with strong relief, whereas the MOLA DTM is often more reliable on level and very smooth terrain as well as on ice surfaces. In the former areas, altimeter heights themselves are even more accurate than for sloping terrain, while stereo image correlation may fail completely if no albedo features or morphologic features are visible.

Further complementarity is related to latitude. It mainly derives from the close spacing of orbit ground tracks at high latitudes, and thus high reliability of the MOLA DTM. In the equatorial zone, MOLA is affected by marked interpolation artifacts that are well represented in differences with HRSC heights. On the contrary, the best HRSC results in terms of resolution, point precision and point density are most often (but not exclusively) found at lower latitudes, while the same parameters show a moderate tendency towards lower precision and coverage for higher latitudes.

In view of the global mapping of Mars by HRSC, we conclude that the necessary techniques are well established and the existing results are encouraging. The goal of global coverage by HRSC high-level data products of course depends on the further progression of the MEX mission. Only few regions on Mars have shown very unfavorable imaging conditions repeatedly in the past.

HRSC represents an example of a novel camera type applied in planetary science. Its built-in stereo capability most naturally leads the focus of interest towards the derived DTM as the primary result of HRSC 3D processing. However, due to their high quality of co-registration with the corresponding DTM, also the orthoimages provide a novel data source that enables new opportunities for 3D analysis in planetary remote sensing.

Acknowledgements

We gratefully acknowledge the support of the participants of the HRSC experiment teams of DLR and Freie Universität Berlin, and of the Mars Express Project teams at ESTEC and ESOC. We also thank for the thoughtful comments by the members of the HRSC Co-Investigator Team, in particular by Marita Wählisch, as well as by an anonymous reviewer and by Gabriele Cremonese.

References

- Albertz, J., Attwenger, M., Barrett, J., Casley, S., Dorninger, P., Dorrer, E., Ebner, H., Gehrke, S., Giese, B., Gwinner, K., Heipke, C., Howington-Kraus, E., Kirk, R.L., Lehmann, H., Mayer, H., Müller, J.-P., Oberst, J., Ostrovskiy, A., Renter, J., Reznik, S., Schmidt, R., Scholten, F., Spiegel, M., Wählisch, M., Neukum, G., the HRSC Co-Investigator Team, 2005. HRSC on Mars Express – photogrammetric and cartographic research. *Photogramm. Eng. Remote Sensing* 71 (10), 1153–1166.
- Greeley, R., Batson, R.M., 1990. *Planetary Mapping: Cambridge Planetary Sciences Series*, vol. 6.

- Grün, A., Zhang, L., 2003. Sensor modelling for aerial triangulation with three-line-scanner (TLS) imagery. *Photogramm. Fernerkund. Geoinf.* 2, 85–98.
- Gwinner, K., Scholten, F., Spiegel, M., Schmidt, R., Giese, B., Oberst, J., Jaumann, R., Neukum, G., the HRSC Co-Investigator Team, 2005. Hochauflösende digitale Geländemodelle auf der Grundlage von Mars Express HRSC-Daten. *Photogramm. Fernerkund. Geoinf.* 5, 387–394.
- Gwinner, K., Roatsch, T., Matz, K.-D., Scholten, F., Elgner, S., Preusker, F., Oberst, J., Jaumann, R., Heather, D., Neukum, G., 2008. Archival stereo data products of the HRSC experiment onboard Mars Express. 39th Lunar and Planetary Science Conference, Houston, Texas (Lunar and Planetary Institute), abstract #2373.
- Gwinner, K., Scholten, F., Spiegel, M., Schmidt, R., Giese, B., Oberst, J., Oberst, J., Jaumann, R., Heipke, C., Neukum, G., 2009. Derivation and validation of high-resolution digital terrain models from Mars Express HRSC-data. *Photogrammetric Engineering and Remote Sensing* 75 (9), 1127–1142.
- Heipke, C., Schmidt, R., Brand, R., Oberst, J., Neukum, G., the HRSC Co-Investigator Team, 2004. Performance of automatic tie point extraction using HRSC imagery of the Mars Express Mission. *Int. Arch. Photogramm. Remote Sens.* XXXV (B4), 846–851.
- Heipke, C., Oberst, J., Albertz, J., Attwenger, M., Dorninger, P., Dorner, E., Ewe, M., Gehrke, S., Gwinner, K., Hirschmüller, H., Kim, J.R., Kirk, R.L., Mayer, H., Müller, J.-P., Rengarajan, R., Rentsch, M., Schmidt, R., Scholten, F., Shan, J., Spiegel, M., Wählich, M., Neukum, G., 2007. Evaluating planetary digital terrain models – the HRSC DTM test. *Planet. Space Sci.* 55, 2173–2191.
- Hoekzema, N., Garcia Comas, M., Petrova, E., Stenzel, O.J., Gwinner, K., Keller, H.U., 2009-this issue. The dust-scale height of the Martian atmosphere in Valles Marineris from HRSC stereo images.
- Hofmann, O., Nave, P., Ebner, H., 1984. DPS – a digital photogrammetric system for producing digital elevation models and orthophotos by means of linear array scanner imagery. *Photogramm. Eng. Remote Sens.* 50 (8), 1135–1142.
- Jaumann, R., Neukum, G., Behnke, T., Duxbury, T.C., Flohrer, J., v. Gasselt, S., Giese, B., Gwinner, K., Hauber, E., Hoffmann, H., Köhler, U., Matz, K.-D., McCord, T.B., Mertens, V., Oberst, J., Pischel, R., Reiss, D., Roatsch, T., Saiger, P., Scholten, F., Schwarz, G., Stephan, K., Wählich, M., 2007. The High Resolution Stereo Camera (HRSC) experiment on Mars Express: instrument aspects and experiment conduct from interplanetary cruise through the nominal mission. *Planet. Space Sci.* 55, 928–952.
- Kirk, R.L., Howington-Kraus, E., Redding, B., Galuszka, D., Hare, T.M., Archinal, B.A., Soderblom, L.A., Barrett, J.M., 2003. High-resolution topomapping of candidate MER landing sites with Mars Orbiter Camera narrow-angle images. *J. Geophys. Res.* 108 (E12). doi:10.1029/2003JE002131.
- Kirk, R.L., Howington-Kraus, E., Galuszka, D., Redding, B., Hare, T.M., 2006. Topomapping of Mars with HRSC images, ISIS, and a commercial stereo workstation. *Int. Arch. Photogramm. Remote Sens.* 36 (4A), 293–298.
- Kirk, R.L., Howington-Kraus, E., Rosiek, M.R., Cook, D., Anderson, J., Becker, K., Archinal, B.A., Keszhelyi, L., King, R., McEwen, A.S., HiRISE Team, 2007. Ultrahigh resolution topographic mapping of Mars with HiRISE stereo images: methods and first results. 38th Lunar and Planetary Science Conference, Houston, Texas (Lunar and Planetary Institute), Abstract #1428.
- Malin, M.C., Edgett, K.S., 2001. Mars global surveyor Mars Orbiter Camera: interplanetary cruise through primary mission. *J. Geophys. Res.* 106 (E10), 23429–23570.
- McEwen, A., Eliason, E., Bergstrom, J., Bridges, N., Hansen, C., Delamere, W., Grant, J., Gulick, V., Herkenhoff, K., Keszhelyi, L., Kirk, R., Mellon, M., Squyres, S., Thomas, N., Weitz, C., 2007. Mars Reconnaissance Orbiters's high resolution imaging science experiment (HiRISE). *J. Geophys. Res.* 112, E05S02. doi:10.1029/2005JE002605.
- Müller, F., 1991. Photogrammetrische Punktbestimmung mit Bilddaten digitaler Dreizeilenkameras. Ph.D. thesis, Deutsche Geodätische Kommission Ser. C, No. 372, Verlag der Bayerischen Akademie der Wissenschaften, Munich, Germany.
- Neukum, G., Jaumann, R., HRSC Co-Investigator Team, 2004. HRSC: the High Resolution Stereo Camera of Mars Express, ESA Special Publications, SP-1240.
- Neumann, G.A., Lemoine, F.G., Smith, D.E., Zuber, M.T., 2003. The Mars Orbiter Laser Altimeter archive: final precision experiment data record release and status of radiometry. 34th Lunar and Planetary Science Conference, Houston, Texas (Lunar and Planetary Institute), Abstract #1778.
- Schmidt, R., Heipke, C., Brand, R., Neukum, G., 2005. Automatische Bestimmung von Verknüpfungspunkten in HRSC-Bildern der Mars Express Mission. *Photogramm. Fernerkund. Geoinf.* 5, 373–379.
- Schmidt, R., 2008. Automatische Bestimmung von Verknüpfungspunkten für HRSC-Bilder der Mars Express-Mission. Ph.D. thesis, DGK C, No. 623, Verlag der Bayerischen Akademie der Wissenschaften, Munich, Germany. (http://129.187.165.2/typo3_dgk/docs/c-623.pdf).
- Schmidt, R., Spiegel, M., Heipke, C., Dumke, A., Neukum, G., HRSC Co-Investigator Team, 2008. Operational determination of tie points and bundle adjustment of HRSC images of the Mars Express Mission. *Int. Arch. Photogramm. Remote Sens.* XXXVII (B4), 1025–1030.
- Scholten, F., Gwinner, K., 2004. Operational parallel processing in digital photogrammetry – strategy and results using different multi-line cameras. *Int. Arch. Photogramm. Remote Sens.* XXXV (B2), 408–413.
- Scholten, F., Gwinner, K., Wewel, F., 2002. Angewandte digitale photogrammetrie mit der HRSC. *Photogramm. Fernerkund. Geoinf.* 5, 317–332.
- Scholten, F., Gwinner, K., Roatsch, T., Matz, K.-D., Wählich, M., Giese, B., Oberst, J., Jaumann, R., Neukum, G., the HRSC Co-Investigator Team, 2005. Mars Express HRSC data processing – methods and operational aspects. *Photogramm. Eng. Remote Sens.* 71 (10), 1143–1152.
- Smith, D.E., Zuber, M.T., Frey, H.V., Garvin, J.B., Head, J.W., 2001. Mars Orbiter Laser Altimeter (MOLA): experiment summary after the first year of global mapping of Mars. *J. Geophys. Res.* 106 (E10), 23689–23722.
- Snyder, C.W., 1979. The extended mission of Viking. *J. Geophys. Res.* 84, 7917–7933.
- Spiegel, M., 2007a. Kombinierte Ausgleichung der Mars Express HRSC Zeilenbilddaten und des Mars Global Surveyor MOLA DGM. Ph.D. thesis, DGK C, No. 610, Verlag der Bayerischen Akademie der Wissenschaften, Munich, Germany (http://129.187.165.2/typo3_dgk/docs/c-610.pdf).
- Spiegel, M., 2007b. Improvement of interior and exterior orientation of the three line camera HRSC with a simultaneous adjustment. *Int. Arch. Photogramm. Remote Sens.* 36 (3/W49B), 161–166.
- Thornhill, G.D., Rothery, D.A., Murray, J.B., Cook, A.C., Day, T., Müller, J.-P., Illife, J.C., 1993. Topography of Apollinaris Patera and Ma'adim Vallis: automated extraction of digital elevation models. *J. Geophys. Res.* 98 (E12), 23581–23587.
- Wu, S., Doyle, F., 1990. Topographic mapping. In: Greeley, R., Batson, R.M. (Eds.), *Planetary Mapping: Cambridge Planetary Sciences Series*, 6, pp. 169–207.
- Yoon, J.S., Shan, J., 2005. Combined adjustment of MOC stereo imagery and MOLA altimetry data. *Photogramm. Eng. Remote Sens.* 71 (10), 1179–1186.